Sfr13, a member of a large family of asymmetrically localized Sfi1-repeat proteins, is important for basal body separation and stability in *Tetrahymena thermophila*

Alexander J. Stemm-Wolf, Janet B. Meehl and Mark Winey*

Department of Molecular, Cellular and Developmental Biology, University of Colorado – Boulder, Boulder, CO 80309, USA

*Author for correspondence (mark.winey@colorado.edu)

Accepted 21 January 2013
Journal of Cell Science 126, 1659–1671

doi: 10.1242/jcs.120238

Summary

Directed fluid flow, which is achieved by the coordinated beating of motile cilia, is required for processes as diverse as cellular swimming, developmental patterning and mucus clearance. Cilia are nucleated, anchored and aligned at the plasma membrane by basal bodies, which are cylindrical microtubule-based structures with ninefold radial symmetry. In the unicellular ciliate *Tetrahymena thermophila*, two centrin family members associated with the basal body are important for both basal body organization and stabilization. We have identified a family of 13 proteins in *Tetrahymena* that contain centrin-binding repeats related to those identified in the *Saccharomyces cerevisiae* Sfi1 protein. We have named these proteins Sfr1–Sfr13 (for Sfi1-repeat). Nine of the Sfr proteins localize in unique polarized patterns surrounding the basal body, suggesting non-identical roles in basal body organization and association with basal body accessory structures. Furthermore, the Sfr proteins are found in distinct basal body populations in *Tetrahymena* cells, indicating that they are responsive to particular developmental programs. A complete genetic deletion of one of the family members, Sfr13, causes unstable basal bodies and defects in daughter basal body separation from the mother, phenotypes also observed with centrin disruption. It is likely that the other Sfr family members are involved in distinct centrin functions, providing specificity to the tasks that centrins perform at basal bodies.

Key words: Centrin, Sfi1-repeat, Asymmetry, Basal body

Introduction

The evolutionarily ancient cylindrical structure known either as the basal body or centriole is important for organizing microtubule-based components of the cytoskeleton (Carvalho-Santos et al., 2011; Hodges et al., 2010). These components include spindle and cytoplasmic microtubules emanating from the centrosome and motile or immotile cilia, which are projections that extend directly from the basal body anchored at the plasma membrane. Although the mitotic spindle, which separates the duplicated genome during cell division, can form in the absence of centrosomes and their centrioles (Doxsey, 2001; Hinchcliffe, 2011), the basal body is absolutely required for cilia formation (Basto et al., 2006). Notably, defects in cilia function are responsible for a number of pleiotropic diseases collectively known as ciliopathies and can have consequences for development, reproduction, signaling pathways and fluid flow (Badano et al., 2006; Baker and Beales, 2009; Bettencourt-Dias et al., 2011).

Both the basal body and centriole are composed predominantly of specialized microtubules, usually triplets, arranged with a ninefold radial symmetry. Assembly is tightly regulated, and generally initiates at an existing organelle (Allen, 1969; Dippell, 1968), although *de novo* assembly occurs in certain cell types and under specific conditions (Hagiwara et al., 2004; Khodjakov et al., 2002; Vorobjev and Chentsov, 1982). Once assembled, tubulin modifications and protein components act to stabilize the structure (Bayless et al., 2012; Bobinnec et al., 1998; Kochanski and Borisy, 1990; Pearson et al., 2009b; Vonderfecht et al., 2011), such that centrioles and basal bodies have the capacity to persist through multiple cell divisions (Nigg and Stearns, 2011; Yamashita and Fuller, 2008) and withstand forces generated by the microtubule structures they anchor (Abal et al., 2005; Bayless et al., 2012).

In addition to the apparent ninefold radial symmetry displayed by centrioles and basal bodies, asymmetric features are also present, particularly with basal bodies. The site of new basal body assembly as well as basal body accessory structures, such as basal feet, kinetodesmal fibers, and basal body associated microtubules, are all positioned at stereotypical locations around the basal body microtubule triplets in a variety of cell types (Allen, 1969; Beisson and Jerka-Dziadosz, 1999; Dippell, 1968; Kunimoto et al., 2012; Wallingford, 2010). Basal body asymmetries may be a heritable property of the basal body itself; when ciliate basal bodies are experimentally rotated 180°, the relative direction and position of new basal body assembly and accessory structures is maintained in the new orientation and passed on to daughter basal bodies through multiple generations (Beisson and Sonneborn, 1965; Ng and Frankel, 1977). This observation suggests that intrinsic differences in the microtubule triplets of the basal body, effects of the local environment near

the basal body or a combination of these factors contribute to the propagation of basal body asymmetries from mother to daughter basal body. These asymmetries, in turn, can have important consequences for cellular organization (Marshall, 2012).

Centrins are small calcium binding proteins that function at centrioles and basal bodies but also in a diverse array of additional activities including nuclear export and DNA damage repair (Chen and Madura, 2008; Fischer et al., 2004; Nishi et al., 2005; Paoletti et al., 1996; Resendes et al., 2008; Yang et al., 2010). Presumably, specificity of localization and function is accomplished through centrin-binding partners. Structural studies of centrin interactions have established that the centrin C-terminal domain includes a hydrophobic pocket capable of interacting with α-helical peptides containing either a Wx2Lx3L sequence motif or inversely related variants (such as Lx3Lx2W) (Azimzadeh et al., 2009; Li et al., 2006; Martinez-Sanz et al., 2006; Martinez-Sanz et al., 2010; Nishi et al., 2005; Thompson et al., 2006). This second motif is found within domains known as 'Sfi1 repeats' (more fully defined as Ax7LLx3F/Lx2WK/R with usually a 33 amino acid periodicity) because they were initially identified in the *Saccharomyces cerevisiae* protein Sfi1 and are required for interaction with the yeast centrin, Cdc31 (Kilmartin, 2003). Sfi1 localizes asymmetrically at the yeast centrosome (termed the spindle pole body, or SPB) and likely plays a critical role in determining when and where SPB assembly occurs (Jaspersen and Winey, 2004; Jones and Winey, 2006; Kilmartin, 2003; Li et al., 2006).

Sequence analysis identified several vertebrate proteins that contain Sfi1-repeats, including one with 23 repeats in the center of the gene similar to yeast Sfi1. This protein localizes to, or very near to centrioles and was named hSfi1, although its function has yet to be determined (Kilmartin, 2003). A second human Sfi1-repeat protein, hPoc5, binds centrin, localizes to the distal end of centrioles and is required for centriole maturation and elongation (Azimzadeh et al., 2009). Large centrin-binding proteins in the ciliate *Paramecium tetraurelia* also contain Sfi1-repeats, and these proteins are required for the centrin-rich infraciliary lattice, a network of calcium responsive contractile fibers that are part of the *Paramecium* cytoskeleton (Gogendeau et al., 2007; Gogendeau et al., 2008).

Tetrahymena thermophila is a ciliate with a highly organized, microtubule based cytoskeleton. Each cell contains ~750 basal bodies, either in cortical rows or in the feeding structure known as the oral apparatus (Frankel, 1999; Wloga and Frankel, 2012). Two centrins, Cen1 (human Cetn2 homologue) and Cen2 (human Cetn3 homologue), reside primarily at basal bodies, and both proteins have populations that localize asymmetrically to the anterior side of the basal body where new basal body assembly is initiated (Stemm-Wolf et al., 2005). Both centrin proteins are required for basal body stability and, like *Paramecium* basal body centrins, for the proper orientation of new basal body assembly (Ruiz et al., 2005; Stemm-Wolf et al., 2005; Vonderfecht et al., 2011; Vonderfecht et al., 2012). To investigate the mechanisms by which centrin affects stability, orientation and asymmetry of basal bodies, an examination of *Tetrahymena* Sfi1-repeat proteins was undertaken.

Results

Sfi1-repeat proteins in *T. thermophila* localize asymmetrically around the basal body

A search of the *Tetrahymena* sequenced genome (Eisen et al., 2006) identified DNA sequences corresponding to 13 predicted Sfi1-repeat containing proteins (with differing numbers of repeats), hereafter referred to as Sfr1–Sfr13 in ascending order of amino acid number (Fig. 1A). Only four of these proteins (Sfr6, Sfr8, Sfr9 and Sfr10) share additional homology, which lies within their N-terminal domains. None of the proteins are close homologs of other known Sfi1-repeat proteins except for Sfr12, which is related to the *Paramecium* CenBPs (supplementary material Fig. S1A) (Gogendeau et al., 2007; Gogendeau et al., 2008). Data from the *Tetrahymena* Genome Expression Database (Miao et al., 2009) indicates that of the 13 Sfr proteins Sfr1 and Sfr10 are the most highly expressed during vegetative growth.

To ascertain whether any of the thirteen predicted proteins localize to basal bodies, all but Sfr1 were endogenously tagged at the C-terminus with mCherry (Day and Davidson, 2009; Shaner et al., 2004) and colocalized with GFP-Poc1 under control of the cadmium inducible *MTT1* promoter (Shang et al., 2002). GFP-Poc1 is known to localize to the basal body proximal end and microtubule scaffold of both cortical row and oral apparatus basal bodies (Pearson et al., 2009b). Due to problems cloning the Sfr1-mCherry construct, N-terminally tagged *MTT1*pr-GFP-Sfr1 was colocalized with endogenously tagged Poc1-mCherry (which accumulates at basal bodies as they mature). Of the thirteen predicted proteins, no localization was observed for two (Sfr2 and Sfr5), although their gene predictions were not tested and confirmed. One (Sfr12) localizes to the fine filamentous reticulum of the oral apparatus and the apical filament band (Fig. 1B, blue arrow and blue arrowhead, respectively), matching localization data for *Tetrahymena* Cen3 (Stemm-Wolf et al., 2005; Wloga and Frankel, 2012) and suggesting that Sfr12 and Cen3 may be binding partners. Furthermore, Sfr12 contains Sfi1-repeats most similar to PtCenBP1 and PtCenBP2 that have features distinct from other Sfi1-repeat proteins, such as the bias for Leucine at position 11 in the 33 amino acid repeat (supplementary material Fig. S1B) (Gogendeau et al., 2007). The ten other Sfr proteins localize to basal bodies, and Sfr4 and Sfr7 also localize to non-basal body structures within the oral apparatus and to the macronucleus (Fig. 1B, yellow arrow) respectively. (Vacuolar signal is the result of background fluorescence in both channels; supplementary material Fig. S1C.) Of the Sfr proteins that specifically localize to basal bodies, only Sfr1 localizes to all basal bodies within the cortical rows and the oral apparatus (Fig. 1B, white arrows indicate basal body structures within the oral apparatus). The others show a surprising specificity for subclasses of basal bodies within the cell. Sfr3, Sfr11 and Sfr13 localize to cortical row basal bodies and to a subset of basal bodies within the oral apparatus corresponding to a substructure called the undulating membrane. Sfr6, Sfr8, Sfr9 and Sfr10, the set of proteins sharing a higher degree of sequence homology, localize primarily to cortical row basal bodies, and colocalization with Poc1 suggests that these proteins are only present at mature (Fig. 1B, white arrowheads) and not new (red arrowheads) basal bodies (magnified in the red-boxed insert). In cells starved for 24 hours where all basal bodies are mature, these four proteins are present at all cortical row basal bodies (supplementary material Fig. S1D), confirming that they are added to basal bodies at a later stage of basal body development. The localization of Sfr proteins to subsets of basal bodies suggests that particular Sfr proteins direct centrin toward specific basal body functions.

The signal from the C-terminally tagged Sfr-mCherry constructs did not completely overlap with the GFP-Poc1

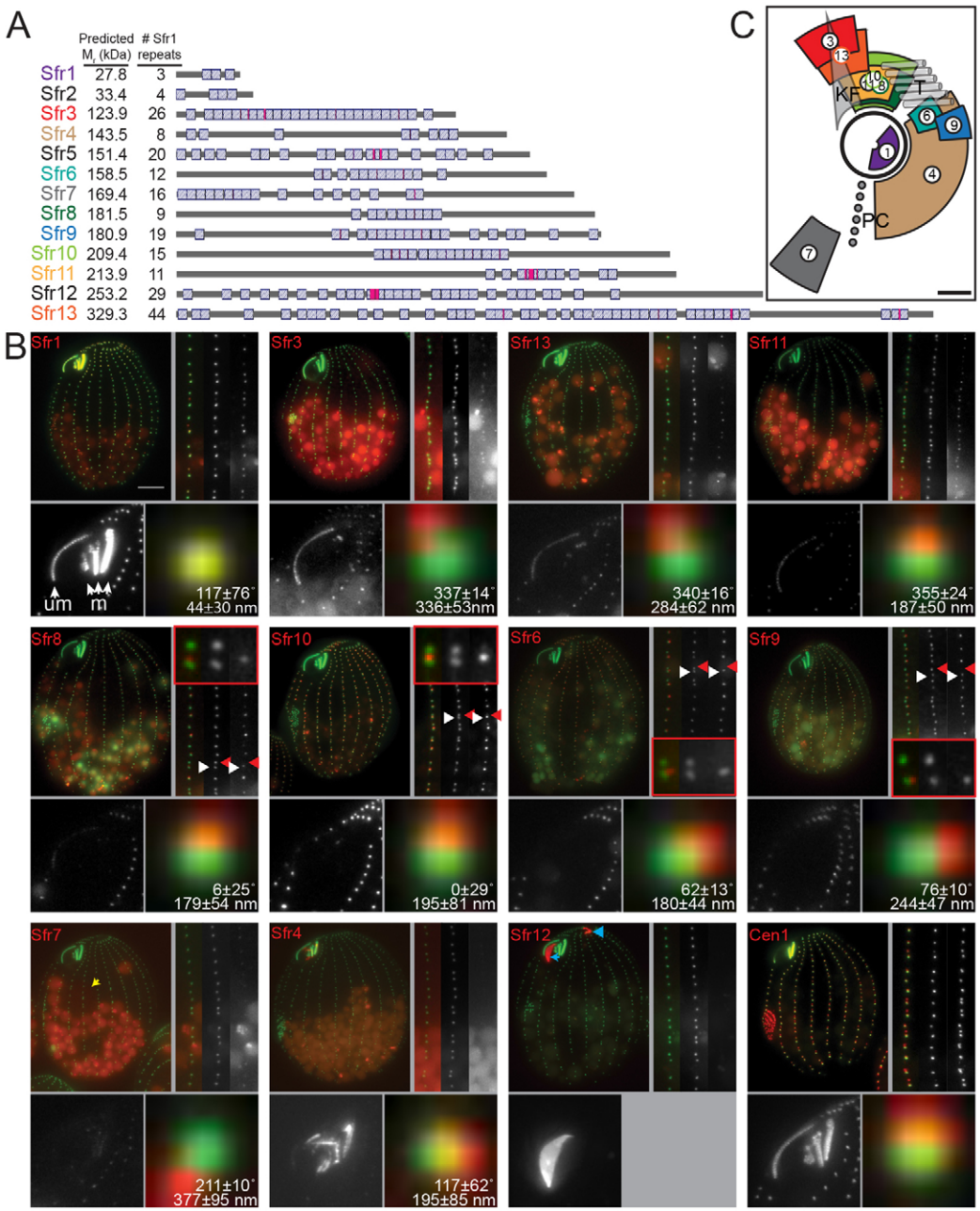

Fig. 1. ***T. thermophila*** **Sfi1-repeat proteins are positioned at specific locations around basal bodies.** (**A**) The 13 Sfi1-repeat predicted proteins identified in the *Tetrahymena* sequenced macronucleus are represented by gray lines, with each 33-amino acid centrin-binding domain displayed as a blue box. Areas where repeats overlap are denoted in pink. The predicted molecular mass and the number of identified repeats are to the left of each schematic. (**B**) Localization of the *Tetrahymena* Sfi1-repeat proteins. The upper left image for each protein shows colocalization of C-terminally mCherry-tagged Sfr protein with N-terminally tagged GFP-Poc1, except for Sfr1 and Cen1, which are N-terminally GFP-tagged and colocalized with C-terminally tagged Poc1-mCherry. All Sfr proteins and Cen1 are displayed in red and Poc1 is displayed in green throughout. The yellow arrow indicates faint macronuclear signal for Sfr7-mCherry. The blue arrow points to fine filamentous reticulum signal for Sfr12, and the blue arrowhead points to Sfr12 staining at apical filament band. The upper right image for each protein consists of three panels that show the merged, Poc1 and Sfr localization (going from left to right) within a cortical row. White arrowheads identify examples of mature basal bodies with both Poc1 and Sfr signal, and red arrowheads indicate new basal bodies without Sfr signal. These basal bodies are also shown enlarged (1.2×2.6 µm) in the red, boxed insets. Each panel is 5×30 µm except where an inset is present where it is 5×20 µm. The lower left image for each protein shows Sfr localization at the oral apparatus. The basal bodies of the undulating membrane (um) and the three membranelles (m) are indicated by the white arrows in the Sfr1 oral apparatus. Panels are 15×15 µm. The lower right image for each protein shows image averages of >45 cortical row basal bodies. The angle (the cells are aligned along the posterior–anterior axis with the anterior at 0°) and distance relative to Poc1 is indicated. Each panel is 0.96×0.96 µm. (**C**) Schematic of the relative positions of the C-termini of the Sfr proteins (except for Sfr1, which was tagged at the N-terminus). The wedges are ±1 s.d. for both the distance and angle from Poc1; the location of the numbered circle indicates the mean position. The black circle represents the basal body diameter of 190 nm. The relative positioning of the kinetodesmal fiber (KF), a segment of the transverse microtubules (T), and the post ciliary microtubules (PC) are shown. Scale bars: 10 µm (B) and 100 nm (C).

signal, suggesting that the C-terminus of many of the Sfr proteins is not at the basal body proper. Image averaging of >45 aligned basal bodies clarified the relative locations of Poc1 and Sfr signals within the X–Y plane (Fig. 1B, lower right panels; supplementary material Fig. S1F). Interestingly, Sfr proteins are distributed asymmetrically around the basal body with different Sfr proteins at distinct locations. For most proteins, the C-terminus is anterior to the basal body (where the site of new basal body assembly and the kinetodesmal fiber and transverse microtubules accessory structures reside) with some angled slightly left (Sfr3, Sfr13), some directly anterior or slightly right (Sfr8, Sfr10, Sfr11) and some far to the right (Sfr6, Sfr9) from the perspective of looking down upon the cell. Two localize posterior to the basal body with one to the right (Sfr4) and the other extending far to the posterior and left (Sfr7) (Fig. 1B,C). GFP-Cen1 colocalization with Poc1-mCherry revealed that this centrin localizes to a broader area than any of the individual Sfr proteins consistent with Cen1 having multiple binding partners primarily to the anterior of the basal body (Fig. 1B; supplementary material Fig. S1E). The repeat domains of Sfi1 form an alpha helix (Li et al., 2006), suggesting that a protein such as Sfr13, which is predicted to be large (329 kDa) and have 44 Sfi1 repeats, could have its N-terminus at the basal body and its C-terminus where it was observed 284 nm away. Of the other asymmetrically localized Sfr proteins, Sfr10 has the highest expression level (Miao et al., 2009), and its exclusive localization to cortical row basal bodies implies a function specific to this subclass of basal bodies (Fig. 1B). Both Sfr10 and Sfr13 have Sfi1-repeats that share the most similarities with the human Sfi1 protein (supplementary material Fig. S1B) (Li et al., 2006) and were examined further. First, cDNAs of Sfr10 and Sfr13 were sequenced; the Sfr10 cDNA sequence matches that of the gene prediction, but differences with the gene prediction were observed for Sfr13 (Fig. 2D), indicating that the protein is 354 kDa and contains 51 Sfi1 repeats (Eisen et al., 2006; Stover et al., 2006).

Sfr proteins direct Cen1 localization

Like yeast Sfi1, Sfr10 has three discrete domains with the N- and C-termini separated by Sfi1-repeats (Fig. 1A). N-terminal GFP fusions were constructed with each domain and placed under the control of the cadmium responsive *MTT1* promoter to identify domains responsible for basal body localization (Fig. 2A). Only cytoplasmic signal was observed for the N-terminal domain. The Sfi1-repeat domain does not localize to basal bodies on its own but instead is surprisingly concentrated at the macronucleus. The lack of basal body localization for the repeat domain suggests that centrin binding does not direct Sfr proteins to basal bodies, but rather Sfr proteins are responsible for centrin's localization to distinct basal body domains. Finally, the C-terminal domain localizes to basal bodies. Interestingly, the basal body localization of the C-terminal domain is different from that of full-length protein. The isolated C-terminal domain localizes to basal bodies, including those in the oral primordium and oral

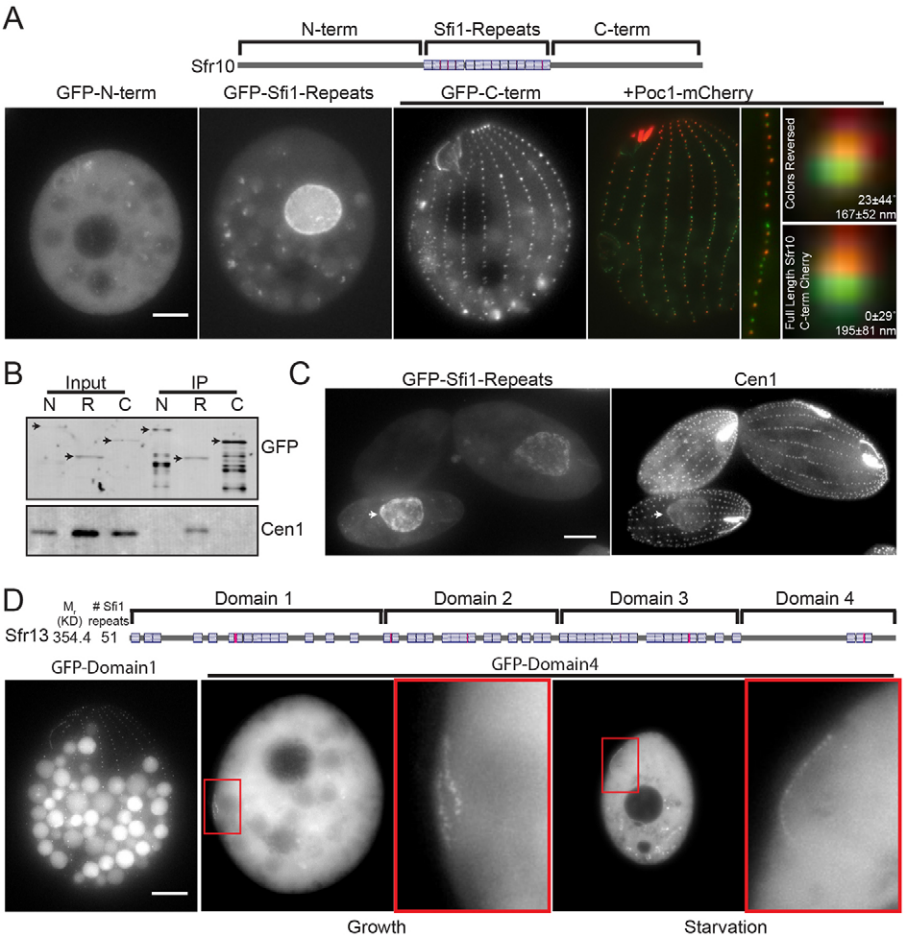

Fig. 2. Sfr10 and Sfr13 domain functions. (**A**) Sfr10 domain localization. Each domain, as shown in the schematic at the top, was fused at its N-terminus with GFP. The C-terminal domain was colocalized with Poc1-mCherry. Basal body signal was averaged from >45 basal bodies. The Sfr10 C-terminus is displayed in red and Poc1 in green and compared with data from C-terminally tagged full-length protein. The angle and distance from Poc1 is indicated. Basal body averaging panels are 0.96×0.96 µm. (**B**) Cen1 interacts with the Sfi1-repeat domain. Immunoprecipitation using a GFP antibody was carried out on extracts from strains bearing the GFP-Sfr10 domain fusions, and a western blot was carried out using GFP and Cen1 antibodies. N, N-terminal domain; R, Sfi1-repeat domain; C, C-terminal domain. Arrows indicate full-length GFP-fusions. (**C**) Cells expressing the GFP-Sfr10 Sfi1-repeat domain were fixed and stained for centrin using the Cen1 antibody. The arrow points to a macronucleus with both Sfi1-repeats and Cen1. (**D**) The Sfr13 N-terminus localizes similarly to full-length protein and the C-terminus localizes specifically to the developing oral apparatus and mature undulating membrane basal bodies. The schematic shows Sfr13 and its domains based on cDNA sequence, including the revised molecular mass and number of Sfi1-repeats. Each domain was fused at its N-terminus to GFP and localization was observed for domain 1 and domain 4. The inserts are 10×15 µm. Scale bars: 10 µm.

apparatus and is not restricted to mature basal bodies within the cortical rows like the full-length protein. To ensure that the C-terminal tag on full-length Sfr10 is not limiting basal body localization to a subset of basal bodies or that overexpression of the C-terminal domain from the *MTT1* promoter is not causing mislocalization to additional basal bodies, an N-terminal mCherry fusion protein under the control of the *MTT1* promoter was generated and found to localize similarly to endogenously expressed C-terminally tagged protein (supplementary material Fig. S2B). Therefore, the limitation of Sfr10 localization solely to cortical row basal bodies is likely provided either by the N-terminal or the repeat domain. Image averaging of the GFP-C-terminal domain colocalized with Poc1-mCherry confirmed that the C-terminal truncation localizes asymmetrically at the basal body similarly to full-length protein. Therefore this protein is anchored to the basal body by its C-terminal domain at this anterior location (Fig. 2A, right panels; supplementary material Fig. S2C).

The Sfr10 GFP-domain fusions were then examined for interactions with centrin. After induction of the fusion proteins, immunoprecipitation was performed using a GFP antibody, and western blots were conducted on the samples using GFP and *Tetrahymena* Cen1 antibodies (Stemm-Wolf et al., 2005). As expected, only the Sfi1-repeat domain interacts with Cen1 (Fig. 2B). Because the Sfi1-repeat domain localizes to the macronucleus, Cen1 localization was monitored in cells expressing this domain to see whether it would be redirected to the macronucleus. Expression of the GFP-Sfi-repeat fusion varied from cell to cell, but increased cellular expression of the fusion protein generated a dose dependent increase in macronuclear localization of Cen1 (Fig. 2C). Furthermore, the GFP-Sfi1-repeat domain expressing strain grows at a slightly slower rate (data not shown), suggesting that the mislocalization of centrin is deleterious to the cells.

A domain analysis similar to that conducted on Sfr10 was performed on Sfr13 by dividing the protein into four domains. Unlike Sfr10, the N-terminal domain of Sfr13 (domain 1) localizes to the same population of basal bodies as full-length protein, albeit with decreased efficiency (Fig. 2D, Fig. 1B; supplementary material Fig. S3A,D). Expression of the C-terminal domain revealed high levels of general cytoplasmic signal and some distinct localization at the oral primordium in growing cells and localization at the oral apparatus, corresponding to the undulating membrane basal bodies, in starved cells (Fig. 2D, right panels). C-terminal domain localization exclusively to the oral apparatus suggests that this protein may have an additional role in organizing oral apparatus basal bodies. Interestingly, Sfr13 is associated with all basal bodies within the developing oral apparatus but as the oral apparatus matures is lost from almost all membranelle basal bodies (supplementary material Fig. S3A,B). Despite repeated attempts, no expression of the two central domains was observed, suggesting that their expression may be deleterious to the cells.

Sfr13 extends from the basal body proper to a site anterior of the basal body

To determine whether Sfr13 has an orientation reminiscent of yeast Sfi1 with its C-terminus projecting away from the microtubule organizing center while the N-terminus is closely associated with it, the location of each terminus in the context of the full length protein was examined. A strain bearing an Sfr13 allele N-terminally tagged with mCherry and under the control of the *MTT1* promoter (supplementary material Fig. S3A), along with the *MTT1* promoter controlled GFP-Poc1, was constructed, and images were taken to observe localization of the two proteins. Image averaging revealed that the two signals do not completely colocalize. The N-terminus, like the C-terminus, is anterior to the basal body, although it is in closer proximity to the basal body than the C-terminus. Comparisons to the C-terminally tagged strain indicate that Sfr13 spans a distance of 167 nm in the X–Y plane and is oriented 39° to the left of the cell posterior–anterior axis (Fig. 3A; supplementary material Fig. S3C). The localization of the N-terminus was confirmed by immuno-electron microscopy on a strain bearing N-terminally tagged GFP-Sfr13 expressed from the *MTT1* promoter using an antibody directed against GFP (Fig. 3B; supplementary material Fig. S3D). A plurality of gold particles (conjugated to the secondary antibody) was observed directly adjacent and anterior to the basal body, which correlates well with the fluorescence data. Localization was also observed at the transition zone and along the microtubule walls, all of which are sites where *Tetrahymena* centrins have been observed (Stemm-Wolf et al., 2005). An attempt to localize the Sfr13 C-terminus by immuno-EM was unsuccessful, probably due to very low expression of the Sfr13-GFP fusion from the Sfr13 endogenous promoter.

Loss of Sfr13 leads to decreased cell growth, small cells and oral apparatus defects

To ascertain the functions of Sfr10 and Sfr13, complete knockout strains were generated (supplementary material Fig. S4A). Surprisingly, the *sfr10Δ* strain had no obvious phenotypes under laboratory conditions when tested for growth, basal body number, basal body organization and cilia generation (data not shown). This may be due to a potential redundancy with *SFR8*, which is a related gene whose product localizes similarly to Sfr10 (Fig. 1B,C; supplementary material Fig. S1A). The *sfr13Δ* strain, on the other hand, is viable, but the growth rate of the cells is reduced by 1.5-fold (Fig. 4A). Furthermore, the *sfr13* deletion leads to a similar reduction in cell volume (Fig. 4B) and in swimming speeds, which were measured at roughly 360 μm per second for wild type and 190 μm per second for the mutant (supplementary material Fig. S4B).

Immunofluorescence microscopy using the Cen1 antibody revealed that the vast majority of *sfr13Δ* cells examined display some degree of gross disorganization of oral apparatus basal bodies (97%, $n=326$ cells), whereas wild-type cells do so rarely (0.5%, $n=198$ cells) (Fig. 4C). The oral apparatus is responsible for sweeping nutrient particles into the oral cavity where they are packaged into vacuoles through phagocytosis. To observe whether this process is impacted by the *sfr13* deletion, the uptake of India ink (Bozzone, 2000; Hoffmann et al., 1974) was monitored at various time points after its introduction to wild-type and *sfr13Δ* cells. While wild-type cells demonstrated steady uptake over 30 minutes, the *sfr13Δ* cells contained fewer and smaller India ink positive vacuoles, corresponding to a roughly 12-fold reduction in phagocytotic nutrient uptake (Fig. 4D; supplementary material Fig. S4C,D). Next, cells were grown in media (EPP) that bypasses the requirement for phagocytosis (Orias and Rasmussen, 1976) to test whether the feeding defect was responsible for the *sfr13Δ* slow growth and reduced size phenotypes. Remarkably, in this media the growth rate for the *sfr13Δ* strain was restored to levels similar to wild type (Fig. 4A). Cell size, however, was unaffected by the media change and

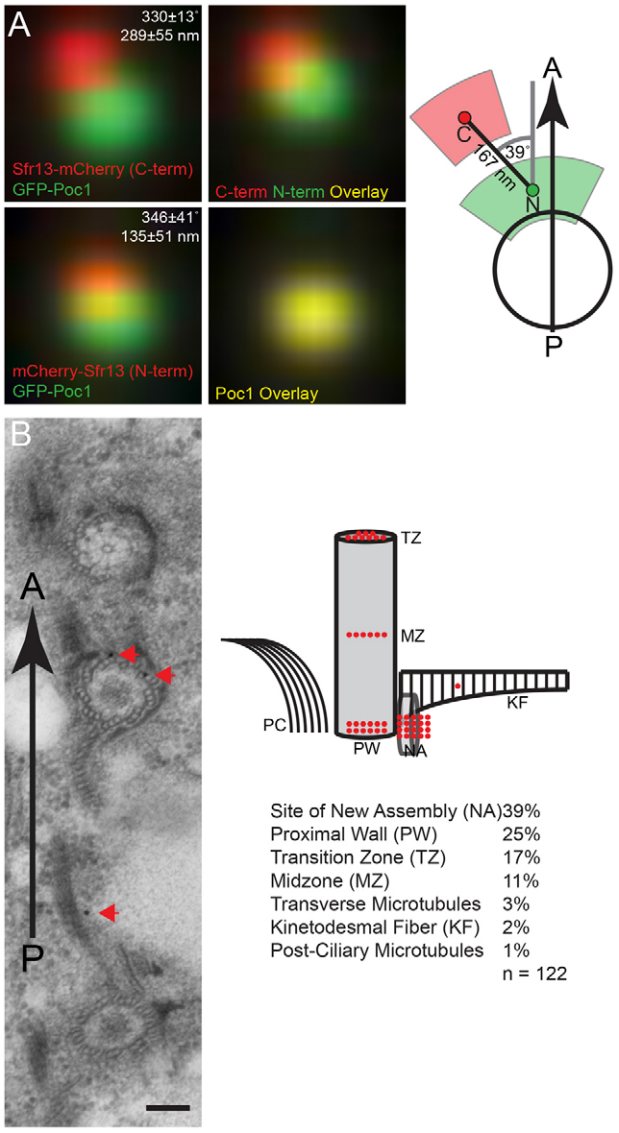

Fig. 3. Sfr13 N-terminus localization. Strains with either Sfr13 N- or C-terminal mCherry were imaged at high magnification along with GFP-Poc1. Basal bodies were averaged (219 from the C-terminally tagged strain and 185 from the N-terminally tagged strain) from seven cells from each strain. The lower right panel shows Poc1 signal from the N- and C-terminally tagged Sfr13 strains overlaid to demonstrate that the images are comparable. The upper right panel shows the N- and C-terminal tags overlaid with each other. Each panel is 1×1 μm. The schematic shows the Sfr13 N- and C-termini ±1 s.d. for both distance and angle with respect to Poc1. The circle represents the 190 nm diameter of the basal body. The arrow indicates the posterior–anterior axis. P, posterior; A, anterior. (**B**) GFP-Sfr13 immuno-electron microscopy. Antibodies against GFP were used to localize N-terminally tagged GFP-Sfr13. Gold particles conjugated to the secondary antibody are indicated by the red arrows. The large arrow shows the posterior–anterior axis. Scale bar: 100 nm. The schematic to the right compiles the data with each red dot representing 2% of the gold particles observed; $n=122$ gold particles.

remained reduced when compared to wild type (Fig. 4B). Furthermore, *sfr13Δ* cells exposed only to EPP media are similarly reduced in cell volume when compared to wild type (data not shown), suggesting that Sfr13 has a distinct role in establishing cell size, perhaps through cytoskeletal organization.

To explore the role of Sfr13 in basal body formation within the highly ordered oral apparatus, the development of new oral apparatuses was examined in the *sfr13Δ* strain. Cells were synchronized and examined by immunofluorescence staining of basal bodies and DNA to monitor progression through the cell cycle. Oral apparatus development was examined within stages from 1a to 5f based on established basal body organizational changes as well as micronuclear morphology (Fig. 4E) (Lansing et al., 1985). Between stages 1b and 3, in wild-type cells there is an expansion in the number of basal bodies in the developing oral apparatus that is much reduced in the *sfr13Δ* strain. The *sfr13Δ* strain proceeds with oral apparatus assembly with fewer basal bodies. Although basal bodies are reorganized in later stages, *sfr13Δ* cells do not generate the third row of basal bodies in the three membranelles or a uniform second column of basal bodies in the undulating membrane. We were unable to determine whether the failed basal body expansion is due to an inability to assemble new basal bodies or due to instability and loss of basal bodies. A third possibility is that in the absence of Sfr13, basal bodies are improperly organized in the developing oral apparatus, and this in turn inhibits basal body assembly. To determine effects Sfr13 may have on basal body assembly and maintenance, cortical row basal bodies were examined in more detail where techniques and markers exist to distinguish between new basal body assembly and basal body maintenance.

Sfr13 promotes daughter basal body separation and reorientation

An analysis of the *sfr13Δ* revealed several cytoskeletal defects beyond those observed in the oral apparatus (Fig. 5A; supplementary material Table S1). The number of basal bodies within 10 μm of each cortical row was slightly lower in the *sfr13Δ* strain (WT=0.83±0.17 basal bodies/μm, *sfr13Δ*=0.78±0.17 basal bodies/μm, $P=0.16$). The cell length was also reduced when compared to wild type (WT=37.17±4.74 μm, *sfr13Δ*=31.97±3.44 μm, $P=2.4\times10^{-7}$). Finally, the number of cortical rows within each cell was reduced (WT=19.53±1.09, *sfr13Δ*=13.63±0.98, $P=2.5\times10^{-29}$). By multiplying these parameters (basal body density (bb/μm)×cell length (μm)×the number of cortical rows (n)), an estimate for the number of cortical row basal bodies can be made. This analysis revealed that the *sfr13Δ* strain has roughly 55% as many basal bodies as wild type in growing cells (Fig. 5A,B, growth 30℃). This defect is due directly to the loss of Sfr13, as a strain bearing a rescuing construct had both normal oral apparatuses (94%, $n=31$ cells), and a normal number of cortical row basal bodies (Fig. 5A 'rescue', B; supplementary material Fig. S4A; Table S1). Centrins in *Tetrahymena* are required for basal body stability (Stemm-Wolf et al., 2005; Vonderfecht et al., 2011; Vonderfecht et al., 2012). To test whether Sfr13 is involved in basal body stability, cells were shifted into starvation media where basal body assembly is eventually suspended but existing basal bodies persist (Pearson et al., 2009a). Cells were starved for 48 hours, and the number of basal bodies was quantified as described above. Between 24 and 48 hours in starvation media, wild-type cells lost on average one basal body each hour. *sfr13Δ* cells lost on average 4.9 basal bodies each hour (Fig. 5A,B; supplementary material Table S1), indicating that Sfr13 contributes substantially to basal body stability.

Because centrin is also important for the proper orientation of basal bodies (Ruiz et al., 2005; Vonderfecht et al., 2011; Vonderfecht et al., 2012), basal body orientation was examined in the *sfr13Δ* strain through an analysis of the angle of the

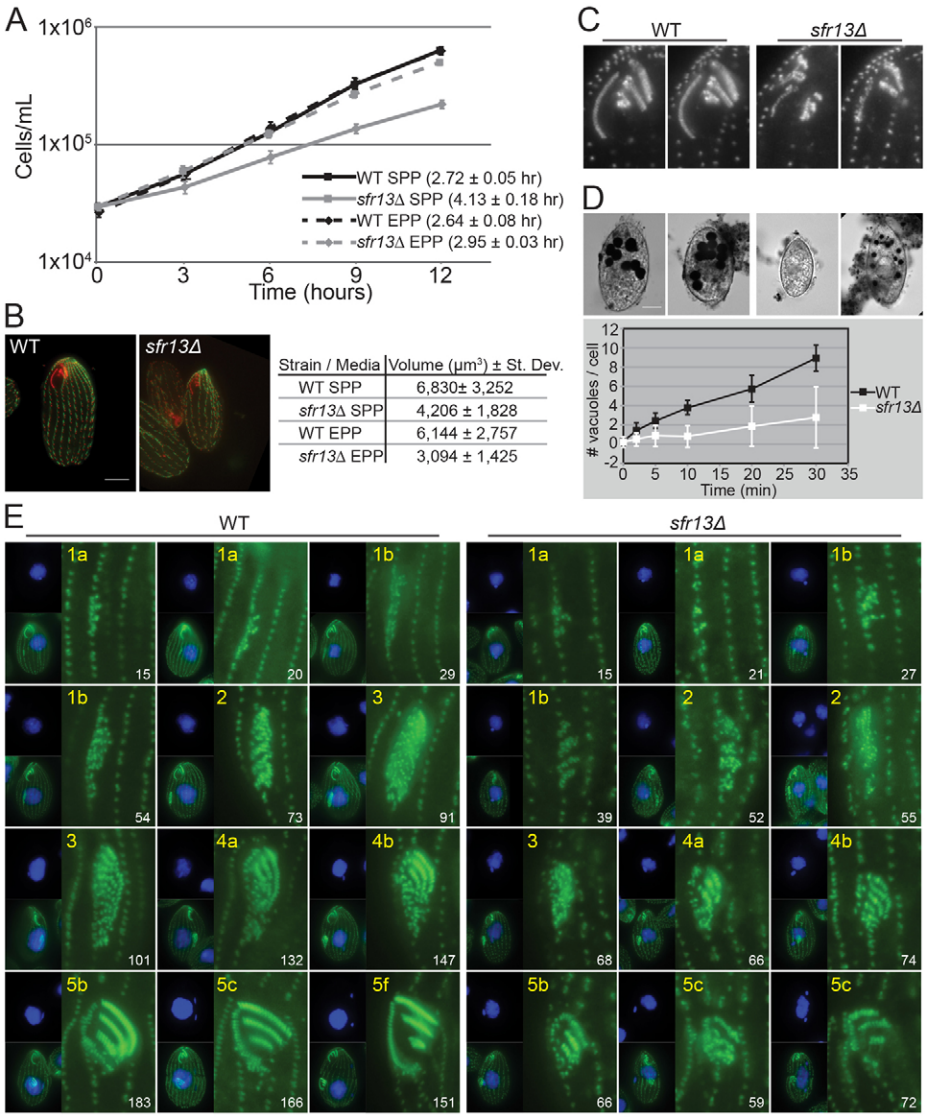

Fig. 4. Deletion of *SFR13* results in growth and oral apparatus defects. (**A**) Growth curves on wild-type and *sfr13Δ* cultures in SPP (standard growth media) and EPP (media that bypasses the need for phagocytosis). The doubling time between 0 and 12 hours was calculated, as indicated in parentheses. Error bars indicate s.d. (**B**) Wild-type and *sfr13Δ* cells stained with antibodies against Cen1 (red) and the kinetodesmal fiber (green). Cell size measurements as calculated by a Coulter Counter are to the right. Scale bar: 10 μm. (**C**) Examples of the oral apparatus from wild-type and *sfr13Δ* cells (Cen1 antibody). Each image is 10×15 μm. (**D**) Oral apparatus function in the *sfr13Δ*. India ink-positive vacuoles were assessed at various time-points. Images are from the 30-minute time-point. Scale bar: 10 μm. The number of India ink positive vacuoles was plotted through time. Error bars indicate s.d.. (**E**) Oral apparatus development. Cells were starved for approximately one doubling time prior to release into EPP media. Oral primordia were imaged using the Cen1 antibody (green) and basal bodies were counted (numbers in white). Oral apparatus development stages (Lansing et al., 1985) are indicated in yellow. Images of oral primordia are 10.7×16.1 μm. Whole cells along with DNA staining (blue) are included on the left to show cell cycle progression.

kinetodesmal fiber relative to the posterior–anterior axis of the cell. The kinetodesmal fiber is a basal body accessory structure that extends towards the cell anterior (Aufderheide et al., 1980; Frankel, 1999). While no defect in basal body orientation was observed in the *sfr13Δ* strain at 30℃ (Fig. 5C), basal body orientation was disordered at 38℃ (WT=356°±10°, *sfr13Δ*=29°±81°). Whether disorder was due to a loss of cytoskeletal organization because of the significant loss of basal bodies or due to improper orientation of new assembly could not be determined by this experiment. Therefore, the orientation of new basal body assembly was assessed in *sfr13Δ* cells. The 10D12 antibody to the K-like protein was used as a marker for old basal bodies, and centrin was used to identify all basal bodies, including newly-assembled basal bodies (Pearson et al., 2009a; Shang et al., 2005; Williams et al., 1990). Cells were grown at 30℃, synchronized at a time prior to cell division when increased basal body assembly occurs (by starvation for approximately one generation time), and released into media at either 30℃ or 38℃. After two hours of release the angle within a cortical row between two mature basal bodies (as determined by the presence of K-like protein) and a new basal body (as determined by the absence of K-like protein) was measured. Only a minor, albeit statistically significant, defect was observed at both 30℃ and 38℃ when comparing wild type to mutant ($P<0.001$ for both). However, there was no significant difference observed when comparing either wild type or mutant between 30℃ and 38℃ ($P=0.81$ and $P=0.13$ respectively) (Fig. 5D,E). Since basal body orientation in the *sfr13Δ* strain is not statistically different from wild type at 30℃ (Fig. 5C), the slight change in angle of new basal body assembly observed at both 30℃ and 38℃ likely does not account for the major basal body orientation defect observed only at 38℃ (Fig. 5C). Therefore, the orientation defect is more probably due to the profound loss of basal bodies observed in the *sfr13* deletion strain at 38℃ (Fig. 5A,B; supplementary material Table S1) and a subsequent loss of cytoskeletal order. This is likely exacerbated during extended growth at elevated temperatures as new basal bodies are assembled from previously misoriented mature basal bodies.

To investigate how Sfr13 functions in basal body stability, cells were starved for 24 hours and then examined by electron microscopy. No obvious basal body disassembly intermediates

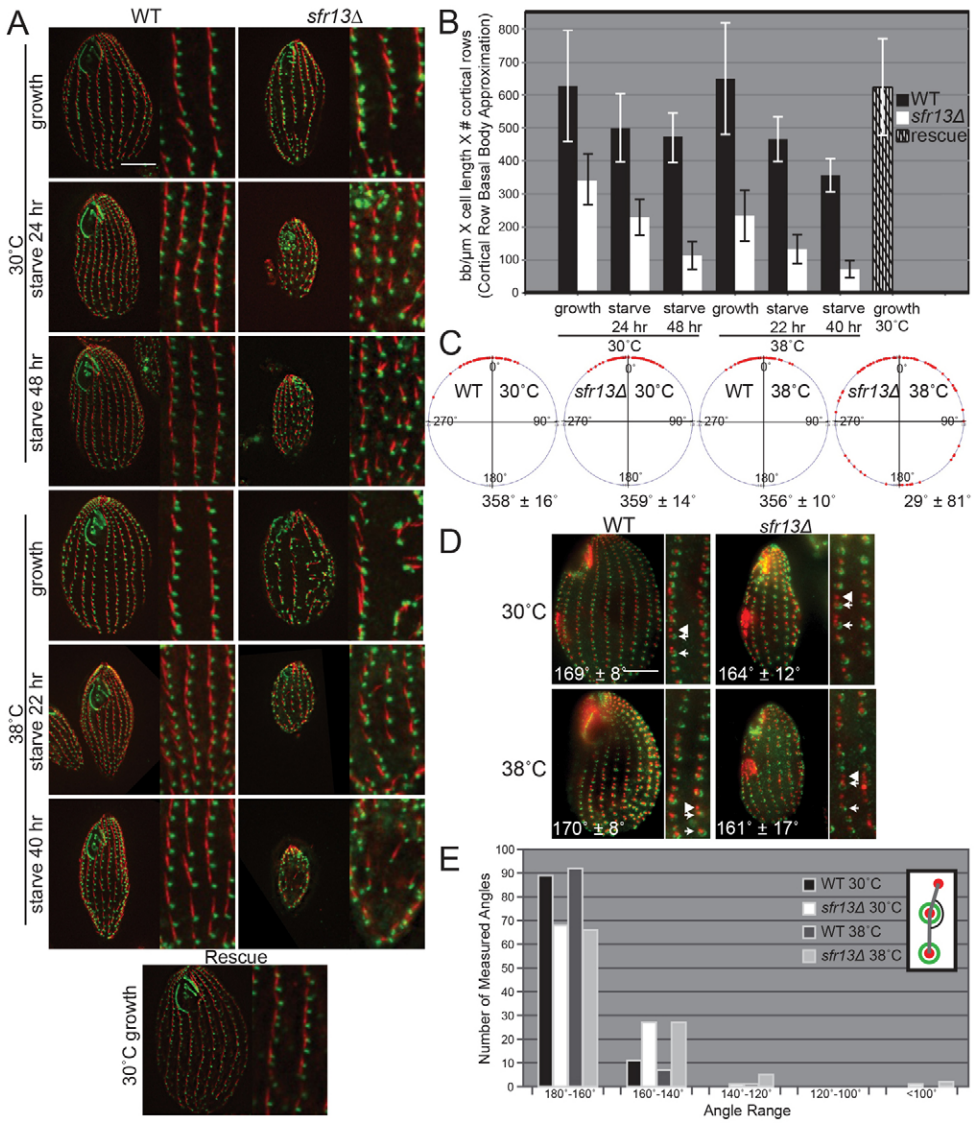

Fig. 5. *SFR13* is required for basal body stability. (**A**) Basal body organization and cellular morphology under different conditions. Cells were stained with Cen1 (green) and kinetodesmal fiber (red) antibodies after growth at 30℃, growth followed by starvation at 30℃, growth at 38℃ or growth at 30℃ followed by starvation at 38℃. Insets are 7.5×15 µm. (**B**) Quantification of cortical row basal bodies. The basal body frequency within cortical rows, cell length and the number of cortical rows were quantified and multiplied to obtain an estimate of the total number of cortical row basal bodies. (For averages and standard deviations for each parameter, see supplementary material Table S1). Error bars indicate s.d. For all 30℃ samples, $n=30$ cells. For 38℃ growth samples, $n=20$ cells. For 38℃ starvation, $n=25$ cells. (**C**) Kinetodesmal fiber angle measurements. Circular plots of angle measurements of the kinetodesmal fibers in wild-type and *sfr13Δ* cells relative to the posterior anterior axis of the cells. Only 100 of the measurements are displayed on each circular plot. The average angle ± s.d. is given below each plot. For wild type at 30℃, $n=535$ angle measurements from 24 cells. For *sfr13Δ* at 30℃, $n=323$ angle measurements from 24 cells. For wild type at 38℃, $n=178$ angle measurements from 10 cells. For *sfr13Δ* at 38℃, $n=246$ angle measurements from 18 cells. (**D**,**E**) Orientation of new basal body assembly. (D) Cells were stained with antibodies to Cen1 (red) to label all basal bodies and K-like (green) to label mature basal bodies. The mean ± s.d. of the angle measurements of newly assembled basal bodies (see the schematic in E) is given in white. The difference between wild type and *sfr13Δ* under each condition is statistically significant using the Student's *t*-test ($P<0.001$), but not statistically significant between *sfr13Δ* at 30℃ and 38℃ ($P=0.13$). Insets are 6×20 µm. $n=100$ angle measurements for each condition, except for *sfr13Δ* at 30℃ where $n=97$ angle measurements. (E) Angle measurements from D were placed into 20° bins and plotted. Scale bars: 10 µm.

were observed. However, several instances in which the daughter basal body had failed to reorient and separate from the mother basal body were seen (Fig. 6A). Daughter basal bodies of this length (318±56 nm, $n=12$ daughter basal bodies observed in starved and growing cells kept at 30℃) are not normally observed perpendicular to the mother basal body, as wild-type daughter basal bodies are already angled 45° relative to the mother basal body when they are 225 nm long (Allen, 1969). To address whether Sfr13 functions in basal body separation, wild type and *sfr13Δ* strains expressing GFP-Poc1 from the *MTT1* promoter were starved for either 5 or 24 hours (to mask effects of new basal body assembly) and imaged. The distance of the fluorescence along the posterior–anterior axis for each punctate signal was measured at half the maximal intensity (to negate

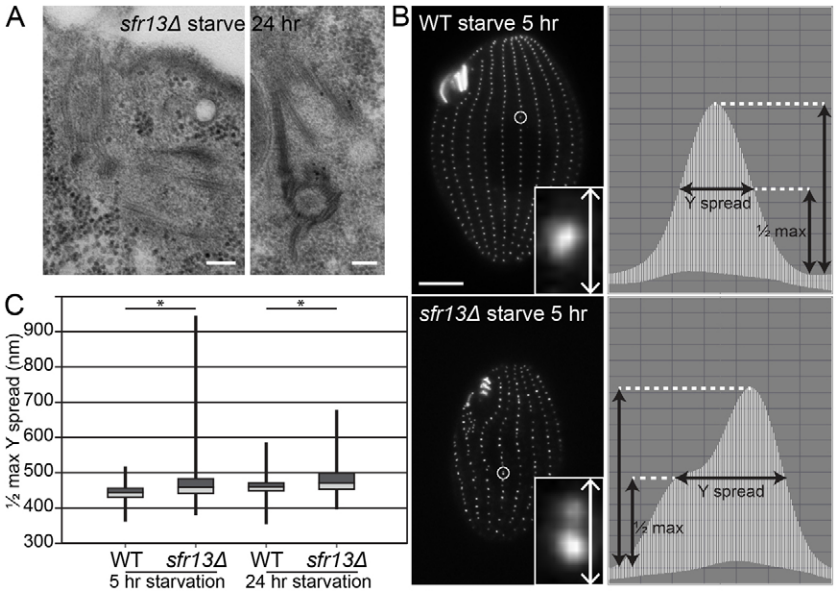

Fig. 6. Sfr13 facilitates basal body reorientation and separation. (**A**) Electron micrographs of the *sfr13Δ* strain starved for 24 hours. The panel on the right is also labeled with the Cen1 antibody. Scale bars: 100 nm. (**B**) GFP-Poc1 signal in wild-type and *sfr13Δ* strains starved for 5 hours. The circled basal bodies are shown in the 0.96×1.5 µm insets. The white arrows indicate the plane of measurements shown in the right panels. Scale bar: 10 µm. (**C**) Box and whisker plots showing the median, first and third quartile, minimum and maximum measurements. The asterisks denote statistical significance of $P<10^{-7}$. For wild type after 5 hours, $n=266$ basal bodies from 6 cells. For *sfr13Δ* after 5 hours, $n=248$ basal bodies from 10 cells. For wild type after 24 hours, $n=145$ basal bodies from 4 cells. For *sfr13Δ* after 24 hours, $n=148$ basal bodies from 5 cells.

effects of changes in fluorescence intensity) (Fig. 6B,C). At both 5 and 24 hours of starvation the fluorescence for the *sfr13Δ* was on average broader than wild type, indicating that Sfr13 plays a role in basal body separation. This offers two possible explanations for the *sfr13Δ* basal body instability phenotype: first, basal bodies that fail to reorient are unable to dock properly at the cell surface leading to their eventual disassembly; second, basal bodies that have failed to separate may appear as one fluorescence spot in immunofluorescence experiments leading to an undercount of basal bodies in the *sfr13Δ* strain.

Discussion

The *Tetrahymena* cell has a highly ordered cytoskeleton in which basal bodies are arranged both in straight cortical rows and within the intricately organized oral apparatus. How the proper basal body arrangement is established is not yet well understood, but it seems likely that different organizational patterns will require different sets of proteins. Centrins, known to have roles in establishing the proper site of basal body assembly and in reorienting and separating basal bodies after assembly (Ruiz et al., 2005; Vonderfecht et al., 2011; Vonderfecht et al., 2012), interact with a number of proteins with the Sfi1 centrin binding domain (Azimzadeh et al., 2009; Gogendeau et al., 2007; Gogendeau et al., 2008; Kilmartin, 2003). It is interesting that many of these Sfr proteins in *Tetrahymena* are limited to specific classes of basal bodies, which leads to the possibility that they are required for specific basal body developmental programs. The related proteins Sfr6, Sfr8, Sfr9 and Sfr10 are present only at mature cortical row basal bodies, while Sfr3, Sfr11 and Sfr13 are present at cortical row basal bodies as well as basal bodies within the undulating membrane substructure of the oral apparatus. Sfr13, which plays an important role in oral apparatus development, is present at all basal bodies in the oral primordium, suggesting that it is involved in the organization of oral apparatus basal bodies prior to its dissociation from the majority of basal bodies within the membranelles.

Sfr proteins not only demonstrate specificity to certain classes of basal bodies but also show specificity in their localization to asymmetric sites around the basal body. These proteins are thus good candidates for partnering with centrin in establishing the geometry and subsequent migration of basal bodies during assembly (a role similar to that proposed for the yeast Sfi1 during spindle pole body duplication (Jones and Winey, 2006; Li et al., 2006)) and individual Sfr proteins may play roles in specific steps of these processes. In addition to its role in the developing oral apparatus, Sfr13 promotes the separation and/or reorientation of new cortical row basal bodies after assembly has been initiated. This phenotype is similar to that reported for the knockdown of *PtCEN3* (Ruiz et al., 2005), and for its homologue, *Tetrahymena CEN2* (Vonderfecht et al., 2012), suggesting that Sfr13 and Cen2 may directly interact with each other. One intriguing possibility is that Sfr13 plays a role in the assembly or function of the newly identified anterior left filament (ALF), which is present at assembling basal bodies, requires *PtCEN3* function in *Paramecium*, and may play a role in daughter basal body positioning (Jerka-Dziadosz et al., 2012). Some centrins and Sfi1 repeat proteins have been found in calcium responsive contractile structures, notably in the infraciliary lattice in *Paramecium* (Gogendeau et al., 2007). The centrin containing nucleus basal body connector in *Chlamydamonas* is also a contractile structure (Geimer and Melkonian, 2004; Wright et al., 1985). Perhaps at *Tetrahymena* basal bodies, a contraction and expansion of Sfr13/Centrin structures serves to reorient and/or shuttle daughter basal bodies away from their mothers. In the absence of this function, basal bodies do not dock at the cell surface efficiently and those that fail in docking are eventually degraded. Sfr13 may also play a more direct role in stabilizing basal bodies, perhaps by distributing forces generated by ciliary beating to the kinetodesmal fiber. As there are multiple Sfr proteins anterior to the basal body, others besides Sfr13 may play a role in the reorientation and positioning of basal bodies and may compensate to some degree for the loss of Sfr13. Sfr proteins may also play a role in establishing the correct site for new basal body assembly as *PtCEN2* does (Ruiz et al., 2005). Therefore, establishing which Sfr proteins interact with which centrins is an important problem worthy of further study. Furthermore, understanding how Sfr proteins localize asymmetrically at the basal body will increase our understanding of the mechanisms underlying the geometry of new basal body assembly.

Whether the functions of centrins (and possible Sfr partners) in the proper orientation of basal body assembly and subsequent migration and reorientation of daughter basal bodies is conserved in metazoans remains to be established. Most metazoan cell types do not possess the highly ordered arrays of basal bodies that are a hallmark of ciliates. Localization of Cetn2 and Cetn3 at human centrioles does not appear to be radially asymmetric, and is limited to the centriolar distal lumen (Paoletti et al., 1996). There is evidence that human centrin may have an important role at basal bodies during ciliogenesis, as centrin levels increase during ciliogenesis in ciliated epithelial cells (Vladar and Stearns, 2007), and depletion of either hCetn2 or hSfi1 results in decreased primary ciliogenesis (Graser et al., 2007). However, centrin localization at these basal bodies remains concentrated at the distal lumen (Laoukili et al., 2000). It will be interesting to see whether centrins affect basal body orientation in multiciliated epithelial cells or in cells aligned by the planar cell polarity pathway.

Morpholinos against zebrafish Centrin 2 resulted in phenotypes including increased tail curvature, small eyes, heart edemas, pronephric cysts and mitotic delays, which are consistent with phenotypes of other mutants known to cause ciliopathies (Delaval et al., 2011). A reduction in cilia number and, importantly, defects in coordinated ciliary beating were also observed. Whether these ciliary defects are the result of an inability of basal bodies to dock at the plasma membrane or orient with each other is unknown, but this is an important question given the roles centrin plays in these processes in ciliates. Furthermore, whether Sfi1-repeat proteins play a role in the polarity of vertebrate basal bodies or play a role with distinct subclasses of basal bodies needs to be established. The discovery of a class of proteins in *Tetrahymena* that display both a range of polarities around basal bodies and specificity for basal body subtypes provides an inroad with which to address these questions.

Materials and Methods

Strains and culture media

Wild type strains included B2086 (from the *Tetrahymena* Stock Center, Cornell University, Ithaca NY), or progeny from a cross between B2086 and CU428 which was used for comparisons with the *sfr13Δ* strain. Cells were grown either at 30℃ or 38℃, in either SPP (Orias et al., 1999) or EPP (Orias and Rasmussen, 1976) as indicated, and starvation was carried out in 10 mM Tris-HCl, pH 7.4. To synchronize cultures, cells were starved for three hours prior to release into EPP media.

Identification of Sfi1-repeat genes

An alignment of 60 Sfi1-repeat domains from *S. cerevisiae*, *S. pombe*, and *H. sapiens* was used for an iterative profile HMM search of the *T. thermophila* sequenced genome translated in six frames using HMMER 2.3.1 (Finn et al., 2011). This identified predicted *Tetrahymena* Sfi1-repeat containing proteins except Sfr6, which was found by a BLAST search using Sfr10 protein sequence, and Sfr12, which was identified by a BLAST search using PtCenBP1 protein sequence.

The Sfr repeat proteins correspond to the following gene predictions: Sfr1=TTHERM_00463380, Sfr2=TTHERM_00925730, Sfr3=TTHERM_00522410, Sfr4=TTHERM_00899420, Sfr5=TTHERM_00466130, Sfr6=TTHERM_00547950, Sfr7=TTHERM_00058810, Sfr8=TTHERM_00059100, Sfr9=TTHERM_00997760, Sfr10=TTHERM_00392670, Sfr11=TTHERM_00421190, Sfr12=TTHERM_00999030, Sfr13=TTHERM_00522830.

Phylogenetic and repeat domain analysis

Phylogenetic analysis was done using the Phylogeny.fr website (Dereeper et al., 2008). Alignments were made using MUSCLE (Edgar, 2004), and the tree was generated using MR.BAYES (Huelsenbeck and Ronquist, 2001), generating 100,000 trees with every 100th sampled and the first 250 discarded. The tree was displayed using TreeDyn (Chevenet et al., 2006). LOGOS to examine the Sfi1-repeat domains were generated using WebLogo (Crooks et al., 2004).

Construction of GFP and mCherry gene fusions

Endogenous C-terminal mCherry fusions were made in the plasmid pmCherryLAP-NEO2 (which is based on p4T2-1 (Gaertig et al., 1994) with the S-peptide, PreScission protease cleavage site and mCherry optimized for expression in *Tetrahymena* followed by sequence downstream of the *MTT1* gene engineered into the plasmid) by integrating 1 kb of the 3′ end of the gene adjacent to the mCherryLAP tag and 1 kb of the 3′ downstream sequence adjacent to the NEO2 selectable marker. Endogenous N-terminal mCherry or GFP fusions were made in pNEO2-MTT1pr-mCherry (which has the *MTT1* promoter followed by mCherry, PreScission protease cleavage site and 6-HIS) or in pNEO2-MTT1pr-GFP (which has EGFP following the *MTT1* promoter) (Winey et al., 2012) in a similar fashion, but using sequences at the 5′ end of the gene. Flanking regions were amplified from genomic DNA using Phusion DNA polymerase (New England Bioloabs, Ipswich, MA). Exogenous N-terminal GFP fusions were made in pBS-MTT-GFP-gtw (Winey et al., 2012). cDNA amplified with SuperScriptII reverse transcriptase (Invitrogen, Grand Island, NY) from DNase treated mRNA followed by amplification with Phusion DNA polymerase (for GFP fusions with Sfr10 and Sfr13 domains) or PCR fragments amplified from genomic DNA were cloned into pENTR4 prior to recombination into pBS-MTT-GFP-gtw using the LR recombinase in the Gateway cloning system (Invitrogen). All transformations take advantage of homologous recombination in *T. thermophila*. Macronuclear transformations were performed using a PDS-1000 particle bombarder (Biorad, Hercules, CA), as previously described (Bruns and Cassidy-Hanley, 1999). 1 μg/ml of $CdCl_2$ was used to induce constructs under the control of the *MTT1* promoter, except for the GFP-Cen1, GFP-Poc1 and GFP-Sfr1 constructs where 0.5 μg/ml of $CdCl_2$ was used.

Fluorescence imaging

Images were collected at room temperature using an Eclipse Ti inverted microscope (Nikon, Japan) fitted with a CFI Plan Apo VC 60× H numerical aperture 1.4 objective (Nikon, Japan) and a CoolSNAP HQ2 charge-coupled device camera (Photometrics, Tuscon, AZ). Metamorph Imaging software (Molecular Devices, Sunnyvale, CA) was used to collect images. The 1.5×intermediate magnification was used for images from Sfr13 N and C-terminal mCherry tags. For live cell imaging, cells were washed once with 10 mM Tris-HCl, pH 7.4, pelleted, and placed on microscope slides (VWR, Radnor, PA).

For immunofluorescence, cells were fixed either by 70% ethanol, 3% formaldehyde, or 3% formaldehyde followed by 15% ethanol (Stuart and Cole, 1999). Antibodies used were *Tetrahymena* Cen1 at 1:2000 (Stemm-Wolf et al., 2005), the kinetodesmal fiber antibody, FI-5D8 at 1:50, and the K-like antibody, FV-10D12 at 1:50 (Shang et al., 2005). Secondary antibodies were anti-rabbit Alexa Fluor 488, anti-mouse Alexa488 (Invitrogen, Grand Island, NY) anti-rabbit Texas Red, and anti-mouse Texas Red (Jackson ImmunoResearch, West Grove, PA) all used at 1:1000. DNA was stained with DAPI at 5 μg/ml. Fixed cells were placed in poly-L-lysine coated multiwelled slides (Polysciences, Inc., Warrington, PA), and antibody incubations were carried out overnight at 4℃ (for primary antibodies), or two hours at room temperature (for secondary antibodies) in PBS+1% BSA with four washes in PBS+0.1% BSA after incubations. Alternatively, antibody incubations were carried out in microcentrifuge tubes and placed on poly-L-lysine coated 18 mm circular coverslips. Cells were mounted in Citifluor (Ted Pella, Inc., Redding, CA).

Image averaging was performed in ImageJ (National Institutes of Health, Bethesda, MD) by placing >15 1×1 μm images of Sfr-mCherry, GFP-Poc1 basal bodies (with the GFP signal centered) in a stack, followed by taking the sum of the stack to create an average image. Image averages from at least three cells were generated in this way, and then averaged to each other. To measure the distances between the peaks of Sfr and Poc1 signal, 3D surface plots of individual basal bodies were made with maximum smoothing, rotated, and the peak signal in the X and Y directions was recorded. The distance between the Sfr and Poc1 peaks was then calculated.

Electron microscopy and immuno-electron microscopy

Tetrahymena cells were prepared for ultrastructural analysis and immunolocalization of Sfr13 by high-pressure freezing followed by freeze substitution (Giddings et al., 2010; Meehl et al., 2009). Cells were centrifuged into a cryoprotectant solution (15% dextran 9–11 kDa and 5% BSA in 2% SPP media). Cells from the loose pellet were loaded into specimen carriers and high-pressure frozen in a Bal-Tec HPM-010 (Leica Microsystems, Wetzlar, Germany), then freeze-substituted in 0.25% glutaraldehyde and 0.1% uranyl acetate in acetone and embedded in Lowicryl HM20.

For immuno-EM formvar-coated nickel grids containing serial 70-nm-thick sections were floated on droplets of blocking solution (2% nonfat dry milk dissolved in PBS containing Tween 20) and then in blocking solution containing the rabbit polyclonal GFP antibody (the gift of Chad Pearson) or the Cen1 antibody (Stemm-Wolf et al., 2005) diluted 1:200 for 2 hours. After rinsing with a stream of PBST, the grids were placed onto droplets containing 15 nm gold-conjugated anti-rabbit

secondary antibody diluted 1:20 in blocking solution (Ted Pella, Redding, CA) followed by rinsing with PBST and a final rinse with water. Grids were poststained with 2% uranyl acetate and lead citrate. Samples were imaged using a Philips CM 100 transmission electron microscope equipped with an AMT V600 digital camera (Advanced Microscopy Techniques, Danvers MA). Basal body profiles were viewed and gold particles were tallied on a diagram to track their distribution. Distance measurements were made using ImageJ.

GFP immunoprecipitations

A polyclonal goat anti-GFP antibody (Rockland Immunochemicals Inc., Gilbertsville, PA) was crosslinked to ProteinG Dynabeads as per manufacturer's instructions (Invitrogen, Grand Island, NY) using dimethyl pimelimidate. Extracts were made following induction of the GFP fusion in 80 mM HEPES 7.4, 1M KCl, 2 mM $MgCl_2$, 2 mM $CaCl_2$, 0.5% Triton X-100, 10% Glycerol, plus protease inhibitors (0.2 mg/ml Soybean Trypsin Inhibitor, 10 µg/ml leupeptin, 1 µg/ml aprotinin, 1 µg/ml pepstatin A, 10 µg/ml TAME, 10 µg/ml benzamidine). Extracts were sonicated six times for 30 seconds with ice incubations in between pulses. The supernatant, after a 10-minute spin at 15,000 rcf at 4℃, was diluted in buffer without KCl such that the final KCl concentration was 150 mM. After an overnight incubation with the anti-GFP beads at 4℃, beads were washed and then eluted with sample buffer. Samples were run in an SDS-polyacrylamide gel and transferred to an Immobilon-P PVDF membrane (EMD Millipore, Billerica, MA), and subjected to western blot with a mouse anti-GFP antibody (Covance, Princeton, NJ), and the rabbit anti-Cen1 antibody (Stemm-Wolf et al., 2005). Secondary antibodies were anti-rabbit Alexa680 (Invitrogen) and anti-mouse IR800, which were detected on a LI-COR Odyssey infrared imager (LI-COR, Lincoln, NE). Incubations were in Tris Buffered Saline with 0.05% Tween 20 and 1% BSA.

Generation of deletion strains

Micronuclear knockout heterokaryons were generated as described previously (Bruns and Cassidy-Hanley, 1999) with the following modifications. The strains used (B2086 and CU428) had the NEO gene with two frame-shift mutations integrated at the RPL29 locus in the macronucleus to counteract DNA elimination of the selectable marker (Mochizuki et al., 2002; Yao et al., 2003), although its usefulness is unclear (Howard-Till and Yao, 2007). Second, after DNA-coated gold particles were introduced during conjugation (using the PDS 1000 from Biorad), the cells were resuspended in Tris-HCl, pH 7.4 for 18 additional hours to allow them to finish conjugation prior to introduction of media. Constructs used to eliminate both *SFR10* or *SFR13* had the NEO2 cassette flanked by 1 kb of sequence upstream of the start codon and 1 kb downstream of the stop codon (Gaertig et al., 1994). Once micronuclear knockout heterokaryons were generated (Hai et al., 1999), strains with different mating types were mated to each other, single mating pairs isolated, and progeny were grown and checked for the complete loss of the wild-type gene by PCR.

India ink uptake

Cells in log phase were resuspended in 10 mM Tris-HCl, pH 7.4 and a 200 µl suspension was mixed with an equal volume of 1% India ink (Super Black India ink, Speedball, Statesville, NC), and 20 µl were added to 10 µl 3% gluteraldehyde at various time points (Bozzone, 2000). Cells were imaged and vacuoles counted using brightfield microscopy. The diameters of India ink positive vacuoles were measured in ImageJ and used to calculate the vacuole volume assuming vacuoles were spherical. A total estimate of India ink uptake for wild-type and *sfr13Δ* strains was made by multiplying the average number of vacuoles to the calculated average vacuole volume at the 30 minute time point.

Calculation of swimming rates, growth rates, and cell size

To determine swimming speeds, cells were grown to mid-log phase and starved for 30 minutes. 15 µl were placed on a slide, and imaged using a 10×plan apo objective (Nikon, Japan) for 1.6 seconds at 0.2-second intervals. The path of each cell was tracked and measured using the freehand line tool in ImageJ. The distance was then divided by the time.

Growth rates were measured for log-phase cultures using a Z2 Coulter Counter (Beckman Coulter, Inc., Indianapolis, IN) over the course of 12 hours. Five independent curves for both wild type and mutant were generated and averaged, using three wild-type and three mutant cell lines. Growth rates were calculated using the 0 and 12-hour timepoints. Cell size was measured on the Z2 Coulter Counter using the Z2 Accucomp software package (Beckman Coulter).

Analysis of cortical row basal bodies

Basal body frequency was measured in ImageJ by counting Cen1 labelled basal bodies within 10 µm of cortical row. For each cell, three cortical rows were examined, two on the side with the oral apparatus, one on the opposite side of the cell. Cell length was also measured using ImageJ. The number of cortical rows was counted within a Z-stack of the entire cell.

Basal body orientation was calculated by measuring the angle of the kinetodesmal fiber when images were aligned such that the posterior–anterior cell axis was vertical using the ImageJ line measurement function. Circular plots were generated using Mathematica software (Wolfram, Champaign, IL). Angle calculations between old and new basal bodies were calculated using the ImageJ angle tool.

Basal body separation analysis was performed in strains transformed with *MTT1pr*-GFP-Poc1. Strains were grown in EPP with 0.025 µg/ml $CdCl_2$ and then starved in media with the same concentration of $CdCl_2$ for either 5 or 24 hours. Images of live cells were collected. 0.96×1.5 µm images of basal bodies were extracted and analyzed in the Y plane (anterior–posterior axis) using the interactive 3D plot function in ImageJ with maximum smoothing. The width of the fluorescent signal was measured at the half maximal intensity.

Statistical analyses were performed in Microsoft Excel (Microsoft Corporation, Redmond, WA), including standard deviation, and the Student's *t*-test.

Rescue strain construction

Because full-length *SFR13* proved too large to clone, a two-step process was used to rescue the *sfr13Δ* strain. The *sfr13Δ* strain was grown (and starved 24 hours prior to transformation) at 30℃. An intermediate strain was made by transformation of the *sfr13Δ* macronucleus with a fragment that spanned from 1 kb upstream to 2 kb after the start codon of *SFR13*, that included a blasticidin resistance cassette for selection (Gaertig and Kapler, 1999). This strain (which behaved like the full knockout) was then transformed with a 9.25 kb fragment that spanned from 1 kb downstream of the start codon to 400 bp downstream of the stop codon. To select for transformants, following the second transformation cells were diluted such that there were ~40 cells per well in fifty 96-well plates, grown for three days in SPP media with 1% proteose peptone, then replica plated into the same media. The following day, cells in wells that grew better were analyzed on the Coulter Counter for cell size. Cultures with wild-type cell size were grown overnight in SPP media to check for a wild-type doubling time. These strains were analyzed by PCR for the knockout, 5′-blasticidin, and wild-type alleles (all three are predicted to be present in the rescue strain macronucleus). Cells were grown for roughly 50 generations before imaging.

Acknowledgements

A profound thanks to Sean Eddy who identified potential Sfi1-repeat genes in the sequenced macronuclear genome. We thank Joseph Frankel for antibodies and Chad Pearson, Shelly Jones and Jennifer Avena for helpful discussions and comments on the manuscript. Jonathan Langberg and Arya Menon contributed to preliminary Sfr13 work.

Author contributions

A.S.-W. conceived and executed all of the experimental work, expect for the electron microscopy, which was performed by J.B.M. M.W. was involved in planning the experimental work and contributed to the manuscript.

Funding

This work was supported by the National Institutes of Health [grant number GM 074746]. Deposited in PMC for release after 12 months.

Supplementary material available online at
http://jcs.biologists.org/lookup/suppl/doi:10.1242/jcs.120238/-/DC1

References

Abal, M., Keryer, G. and Bornens, M. (2005). Centrioles resist forces applied on centrosomes during G2/M transition. *Biol. Cell* **97**, 425-434.

Allen, R. D. (1969). The morphogenesis of basal bodies and accessory structures of the cortex of the ciliated protozoan *Tetrahymena pyriformis*. *J. Cell Biol.* **40**, 716-733.

Aufderheide, K. J., Frankel, J. and Williams, N. E. (1980). Formation and positioning of surface-related structures in protozoa. *Microbiol. Rev.* **44**, 252-302.

Azimzadeh, J., Hergert, P., Delouvée, A., Euteneuer, U., Formstecher, E., Khodjakov, A. and Bornens, M. (2009). hPOC5 is a centrin-binding protein required for assembly of full-length centrioles. *J. Cell Biol.* **185**, 101-114.

Badano, J. L., Mitsuma, N., Beales, P. L. and Katsanis, N. (2006). The ciliopathies: an emerging class of human genetic disorders. *Annu. Rev. Genomics Hum. Genet.* **7**, 125-148.

Baker, K. and Beales, P. L. (2009). Making sense of cilia in disease: the human ciliopathies. *Am. J. Med. Genet. C. Semin. Med. Genet.* **151C**, 281-295.

Basto, R., Lau, J., Vinogradova, T., Gardiol, A., Woods, C. G., Khodjakov, A. and Raff, J. W. (2006). Flies without centrioles. *Cell* **125**, 1375-1386.

Bayless, B. A., Giddings, T. H., Jr, Winey, M. and Pearson, C. G. (2012). Bld10/Cep135 stabilizes basal bodies to resist cilia-generated forces. *Mol. Biol. Cell* **23**, 4820-4832.

Beisson, J. and Jerka-Dziadosz, M. (1999). Polarities of the centriolar structure: morphogenetic consequences. *Biol. Cell* **91**, 367-378.
Beisson, J. and Sonneborn, T. M. (1965). Cytoplasmic inheritance of the organization of the cell cortex in *Paramecium aurelia*. *Proc. Natl. Acad. Sci. USA* **53**, 275-282.
Bettencourt-Dias, M., Hildebrandt, F., Pellman, D., Woods, G. and Godinho, S. A. (2011). Centrosomes and cilia in human disease. *Trends Genet.* **27**, 307-315.
Bobinnec, Y., Khodjakov, A., Mir, L. M., Rieder, C. L., Eddé, B. and Bornens, M. (1998). Centriole disassembly in vivo and its effect on centrosome structure and function in vertebrate cells. *J. Cell Biol.* **143**, 1575-1589.
Bozzone, D. M. (2000). Investigating phagocytosis in *"Tetrahymena"*: an experimental system suitable for introductory and advanced instruction. *Am. Biol. Teach.* **62**, 136-139.
Bruns, P. J. and Cassidy-Hanley, D. (1999). Biolistic transformation of macro- and micronuclei. *Methods Cell Biol.* **62**, 501-512.
Carvalho-Santos, Z., Azimzadeh, J., Pereira-Leal, J. B. and Bettencourt-Dias, M. (2011). Evolution: Tracing the origins of centrioles, cilia, and flagella. *J. Cell Biol.* **194**, 165-175.
Chen, L. and Madura, K. (2008). Centrin/Cdc31 is a novel regulator of protein degradation. *Mol. Cell. Biol.* **28**, 1829-1840.
Chevenet, F., Brun, C., Bañuls, A.-L., Jacq, B. and Christen, R. (2006). TreeDyn: towards dynamic graphics and annotations for analyses of trees. *BMC Bioinformatics* **7**, 439.
Crooks, G. E., Hon, G., Chandonia, J.-M. and Brenner, S. E. (2004). WebLogo: a sequence logo generator. *Genome Res.* **14**, 1188-1190.
Day, R. N. and Davidson, M. W. (2009). The fluorescent protein palette: tools for cellular imaging. *Chem. Soc. Rev.* **38**, 2887-2921.
Delaval, B., Covassin, L., Lawson, N. D. and Doxsey, S. (2011). Centrin depletion causes cyst formation and other ciliopathy-related phenotypes in zebrafish. *Cell Cycle* **10**, 3964-3972.
Dereeper, A., Guignon, V., Blanc, G., Audic, S., Buffet, S., Chevenet, F., Dufayard, J.-F., Guindon, S., Lefort, V., Lescot, M. et al. (2008). Phylogeny.fr: robust phylogenetic analysis for the non-specialist. *Nucleic Acids Res.* **36**, W465-W469.
Dippell, R. V. (1968). The development of basal bodies in *Paramecium*. *Proc. Natl. Acad. Sci. USA* **61**, 461-468.
Doxsey, S. (2001). Re-evaluating centrosome function. *Nat. Rev. Mol. Cell Biol.* **2**, 688-698.
Edgar, R. C. (2004). MUSCLE: multiple sequence alignment with high accuracy and high throughput. *Nucleic Acids Res.* **32**, 1792-1797.
Eisen, J. A., Coyne, R. S., Wu, M., Wu, D., Thiagarajan, M., Wortman, J. R., Badger, J. H., Ren, Q., Amedeo, P., Jones, K. M. et al. (2006). Macronuclear genome sequence of the ciliate *Tetrahymena thermophila*, a model eukaryote. *PLoS Biol.* **4**, e286.
Finn, R. D., Clements, J. and Eddy, S. R. (2011). HMMER web server: interactive sequence similarity searching. *Nucleic Acids Res.* **39 Suppl. 2**, W29-W37.
Fischer, T., Rodríguez-Navarro, S., Pereira, G., Rácz, A., Schiebel, E. and Hurt, E. (2004). Yeast centrin Cdc31 is linked to the nuclear mRNA export machinery. *Nat. Cell Biol.* **6**, 840-848.
Frankel, J. (1999). Cell biology of *Tetrahymena thermophila*. *Methods Cell Biol.* **62**, 27-125.
Gaertig, J. and Kapler, G. (1999). Transient and stable DNA transformation of *Tetrahymena thermophila* by electroporation. *Methods Cell Biol.* **62**, 485-500.
Gaertig, J., Gu, L., Hai, B. and Gorovsky, M. A. (1994). High frequency vector-mediated transformation and gene replacement in *Tetrahymena*. *Nucleic Acids Res.* **22**, 5391-5398.
Geimer, S. and Melkonian, M. (2004). The ultrastructure of the *Chlamydomonas reinhardtii* basal apparatus: identification of an early marker of radial asymmetry inherent in the basal body. *J. Cell Sci.* **117**, 2663-2674.
Giddings, T. H., Jr, Meehl, J. B., Pearson, C. G. and Winey, M. (2010). Electron tomography and immuno-labeling of *Tetrahymena thermophila* basal bodies. *Methods Cell Biol.* **96**, 117-141.
Gogendeau, D., Beisson, J., de Loubresse, N. G., Le Caer, J.-P., Ruiz, F., Cohen, J., Sperling, L., Koll, F. and Klotz, C. (2007). An Sfi1p-like centrin-binding protein mediates centrin-based Ca2+-dependent contractility in *Paramecium tetraurelia*. *Eukaryot. Cell* **6**, 1992-2000.
Gogendeau, D., Klotz, C., Arnaiz, O., Malinowska, A., Dadlez, M., de Loubresse, N. G., Ruiz, F., Koll, F. and Beisson, J. (2008). Functional diversification of centrins and cell morphological complexity. *J. Cell Sci.* **121**, 65-74.
Graser, S., Stierhof, Y.-D., Lavoie, S. B., Gassner, O. S., Lamla, S., Le Clech, M. and Nigg, E. A. (2007). Cep164, a novel centriole appendage protein required for primary cilium formation. *J. Cell Biol.* **179**, 321-330.
Hagiwara, H., Ohwada, N. and Takata, K. (2004). Cell biology of normal and abnormal ciliogenesis in the ciliated epithelium. *Int. Rev. Cytol.* **234**, 101-141.
Hai, B., Gaertig, J. and Gorovsky, M. A. (1999). Knockout heterokaryons enable facile mutagenic analysis of essential genes in *Tetrahymena*. *Methods Cell Biol.* **62**, 513-531.
Hinchcliffe, E. H. (2011). The centrosome and bipolar spindle assembly: does one have anything to do with the other? *Cell Cycle* **10**, 3841-3848.
Hodges, M. E., Scheumann, N., Wickstead, B., Langdale, J. A. and Gull, K. (2010). Reconstructing the evolutionary history of the centriole from protein components. *J. Cell Sci.* **123**, 1407-1413.
Hoffmann, E. K., Rasmussen, L. and Zeuthen, E. (1974). Cytochalasin B: aspects of phagocytosis in nutrient uptake in *Tetrahymena*. *J. Cell Sci.* **15**, 403-406.
Howard-Till, R. A. and Yao, M.-C. (2007). Tudor nuclease genes and programmed DNA rearrangements in *Tetrahymena thermophila*. *Eukaryot. Cell* **6**, 1795-1804.
Huelsenbeck, J. P. and Ronquist, F. (2001). MRBAYES: Bayesian inference of phylogenetic trees. *Bioinformatics* **17**, 754-755.
Jaspersen, S. L. and Winey, M. (2004). The budding yeast spindle pole body: structure, duplication, and function. *Annu. Rev. Cell Dev. Biol.* **20**, 1-28.
Jerka-Dziadosz, M., Koll, F., Włoga, D., Gogendeau, D., Garreau de Loubresse, N., Ruiz, F., Fabczak, S. and Beisson, J. (2012). A centrin3-dependent, transient, appendage of the mother basal body guides the positioning of the daughter basal body in *Paramecium*. *Protist*. [Epub ahead of print].
Jones, M. H. and Winey, M. (2006). Centrosome duplication: is asymmetry the clue? *Curr. Biol.* **16**, R808-R810.
Khodjakov, A., Rieder, C. L., Sluder, G., Cassels, G., Sibon, O. and Wang, C.-L. (2002). De novo formation of centrosomes in vertebrate cells arrested during S phase. *J. Cell Biol.* **158**, 1171-1181.
Kilmartin, J. V. (2003). Sfi1p has conserved centrin-binding sites and an essential function in budding yeast spindle pole body duplication. *J. Cell Biol.* **162**, 1211-1221.
Kochanski, R. S. and Borisy, G. G. (1990). Mode of centriole duplication and distribution. *J. Cell Biol.* **110**, 1599-1605.
Kunimoto, K., Yamazaki, Y., Nishida, T., Shinohara, K., Ishikawa, H., Hasegawa, T., Okanoue, T., Hamada, H., Noda, T., Tamura, A. et al. (2012). Coordinated ciliary beating requires Odf2-mediated polarization of basal bodies via basal feet. *Cell* **148**, 189-200.
Lansing, T. J., Frankel, J. and Jenkins, L. M. (1985). Oral ultrastructure and oral development of the misaligned undulating membrane mutant of *Tetrahymena thermophila*. *J. Protozool.* **32**, 126-139.
Laoukili, J., Perret, E., Middendorp, S., Houcine, O., Guennou, C., Marano, F., Bornens, M. and Tournier, F. (2000). Differential expression and cellular distribution of centrin isoforms during human ciliated cell differentiation in vitro. *J. Cell Sci.* **113**, 1355-1364.
Li, S., Sandercock, A. M., Conduit, P., Robinson, C. V., Williams, R. L. and Kilmartin, J. V. (2006). Structural role of Sfi1p-centrin filaments in budding yeast spindle pole body duplication. *J. Cell Biol.* **173**, 867-877.
Marshall, W. F. (2012). Centriole asymmetry determines algal cell geometry. *Curr. Opin. Plant Biol.* **15**, 632-637.
Martinez-Sanz, J., Yang, A., Blouquit, Y., Duchambon, P., Assairi, L. and Craescu, C. T. (2006). Binding of human centrin 2 to the centrosomal protein hSfi1. *FEBS J.* **273**, 4504-4515.
Martinez-Sanz, J., Kateb, F., Assairi, L., Blouquit, Y., Bodenhausen, G., Abergel, D., Mouawad, L. and Craescu, C. T. (2010). Structure, dynamics and thermodynamics of the human centrin 2/hSfi1 complex. *J. Mol. Biol.* **395**, 191-204.
Meehl, J. B., Giddings, T. H., Jr and Winey, M. (2009). High pressure freezing, electron microscopy, and immuno-electron microscopy of *Tetrahymena thermophila* basal bodies. *Methods Mol. Biol.* **586**, 227-241.
Miao, W., Xiong, J., Bowen, J., Wang, W., Liu, Y., Braguinets, O., Grigull, J., Pearlman, R. E., Orias, E. and Gorovsky, M. A. (2009). Microarray analyses of gene expression during the *Tetrahymena thermophila* life cycle. *PLoS ONE* **4**, e4429.
Mochizuki, K., Fine, N. A., Fujisawa, T. and Gorovsky, M. A. (2002). Analysis of a piwi-related gene implicates small RNAs in genome rearrangement in *Tetrahymena*. Cell ***110****, 689-699.*
Ng, S. F. and Frankel, J. (1977). 180 degrees rotation of ciliary rows and its morphogenetic implications in *Tetrahymena pyriformis*. *Proc. Natl. Acad. Sci. USA* **74**, 1115-1119.
Nigg, E. A. and Stearns, T. (2011). The centrosome cycle: Centriole biogenesis, duplication and inherent asymmetries. *Nat. Cell Biol.* **13**, 1154-1160.
Nishi, R., Okuda, Y., Watanabe, E., Mori, T., Iwai, S., Masutani, C., Sugasawa, K. and Hanaoka, F. (2005). Centrin 2 stimulates nucleotide excision repair by interacting with xeroderma pigmentosum group C protein. *Mol. Cell. Biol.* **25**, 5664-5674.
Orias, E. and Rasmussen, L. (1976). Dual capacity for nutrient uptake in *Tetrahymena*. IV. Growth without food vacuoles and its implications. *Exp. Cell Res.* **102**, 127-137.
Orias, E., Hamilton, E. P. and Orias, J. D. (1999). *Tetrahymena* as a laboratory organism: useful strains, cell culture, and cell line maintenance. *Methods Cell Biol.* **62**, 189-211.
Paoletti, A., Moudjou, M., Paintrand, M., Salisbury, J. L. and Bornens, M. (1996). Most of centrin in animal cells is not centrosome-associated and centrosomal centrin is confined to the distal lumen of centrioles. *J. Cell Sci.* **109**, 3089-3102.
Pearson, C. G., Giddings, T. H., Jr and Winey, M. (2009a). Basal body components exhibit differential protein dynamics during nascent basal body assembly. *Mol. Biol. Cell* **20**, 904-914.
Pearson, C. G., Osborn, D. P. S., Giddings, T. H., Jr, Beales, P. L. and Winey, M. (2009b). Basal body stability and ciliogenesis requires the conserved component Poc1. *J. Cell Biol.* **187**, 905-920.
Resendes, K. K., Rasala, B. A. and Forbes, D. J. (2008). Centrin 2 localizes to the vertebrate nuclear pore and plays a role in mRNA and protein export. *Mol. Cell. Biol.* **28**, 1755-1769.
Ruiz, F., Garreau de Loubresse, N., Klotz, C., Beisson, J. and Koll, F. (2005). Centrin deficiency in *Paramecium* affects the geometry of basal-body duplication. *Curr. Biol.* **15**, 2097-2106.
Shaner, N. C., Campbell, R. E., Steinbach, P. A., Giepmans, B. N. G., Palmer, A. E. and Tsien, R. Y. (2004). Improved monomeric red, orange and yellow fluorescent proteins derived from *Discosoma* sp. red fluorescent protein. *Nat. Biotechnol.* **22**, 1567-1572.

Shang, Y., Song, X., Bowen, J., Corstanje, R., Gao, Y., Gaertig, J. and Gorovsky, M. A. (2002). A robust inducible-repressible promoter greatly facilitates gene knockouts, conditional expression, and overexpression of homologous and heterologous genes in *Tetrahymena thermophila*. *Proc. Natl. Acad. Sci. USA* **99**, 3734-3739.

Shang, Y., Tsao, C.-C. and Gorovsky, M. A. (2005). Mutational analyses reveal a novel function of the nucleotide-binding domain of gamma-tubulin in the regulation of basal body biogenesis. *J. Cell Biol.* **171**, 1035-1044.

Stemm-Wolf, A. J., Morgan, G., Giddings, T. H., Jr, White, E. A., Marchione, R., McDonald, H. B. and Winey, M. (2005). Basal body duplication and maintenance require one member of the *Tetrahymena thermophila* centrin gene family. *Mol. Biol. Cell* **16**, 3606-3619.

Stover, N. A., Krieger, C. J., Binkley, G., Dong, Q., Fisk, D. G., Nash, R., Sethuraman, A., Weng, S. and Cherry, J. M. (2006). *Tetrahymena* Genome Database (TGD): a new genomic resource for *Tetrahymena thermophila* research. *Nucleic Acids Res.* **34 Database issue**, D500-D503.

Stuart, K. R. and Cole, E. S. (1999). Nuclear and cytoskeletal fluorescence microscopy techniques. *Methods Cell Biol.* **62**, 291-311.

Thompson, J. R., Ryan, Z. C., Salisbury, J. L. and Kumar, R. (2006). The structure of the human centrin 2-xeroderma pigmentosum group C protein complex. *J. Biol. Chem.* **281**, 18746-18752.

Vladar, E. K. and Stearns, T. (2007). Molecular characterization of centriole assembly in ciliated epithelial cells. *J. Cell Biol.* **178**, 31-42.

Vonderfecht, T., Stemm-Wolf, A. J., Hendershott, M., Giddings, T. H., Jr, Meehl, J. B. and Winey, M. (2011). The two domains of centrin have distinct basal body functions in *Tetrahymena*. *Mol. Biol. Cell* **22**, 2221-2234.

Vonderfecht, T., Cookson, M. W., Giddings, T. H., Jr, Clarissa, C. and Winey, M. (2012). The two human centrin homologues have similar but distinct functions at *Tetrahymena* basal bodies. *Mol. Biol. Cell* **23**, 4766-4777.

Vorobjev, I. A. and Chentsov, Yu. S. (1982). Centrioles in the cell cycle. I. Epithelial cells. *J. Cell Biol.* **93**, 938-949.

Wallingford, J. B. (2010). Planar cell polarity signaling, cilia and polarized ciliary beating. *Curr. Opin. Cell Biol.* **22**, 597-604.

Williams, N. E., Honts, J. E. and Kaczanowska, J. (1990). The formation of basal body domains in the membrane skeleton of *Tetrahymena*. *Development* **109**, 935-942.

Winey, M., Stemm-Wolf, A. J., Giddings, T. H., Jr and Pearson, C. G. (2012). Cytological analysis of *Tetrahymena thermophila*. *Methods Cell Biol.* **109**, 357-378.

Wloga, D. and Frankel, J. (2012). From molecules to morphology: cellular organization of *Tetrahymena thermophila*. *Methods Cell Biol.* **109**, 83-140.

Wright, R. L., Salisbury, J. and Jarvik, J. W. (1985). A nucleus-basal body connector in *Chlamydomonas reinhardtii* that may function in basal body localization or segregation. *J. Cell Biol.* **101**, 1903-1912.

Yamashita, Y. M. and Fuller, M. T. (2008). Asymmetric centrosome behavior and the mechanisms of stem cell division. *J. Cell Biol.* **180**, 261-266.

Yang, C.-H., Kasbek, C., Majumder, S., Yusof, A. M. and Fisk, H. A. (2010). Mps1 phosphorylation sites regulate the function of centrin 2 in centriole assembly. *Mol. Biol. Cell* **21**, 4361-4372.

Yao, M.-C., Fuller, P. and Xi, X. (2003). Programmed DNA deletion as an RNA-guided system of genome defense. *Science* **300**, 1581-1584.